

Theory of double resonance magnetometers based on atomic alignment

Antoine Weis and Georg Bison

Physics Department, University of Fribourg, Chemin du Musée 3, 1700 Fribourg, Switzerland

Anatoly S. Pazgalev

Physics Department, University of Fribourg, Chemin du Musée 3, 1700 Fribourg, Switzerland and
Io e Physical Technical Institute, Russ. Acad. Sc., St. Petersburg, 194021, Russia

(Dated: May 26, 2006)

We present a theoretical study of the spectra produced by optical/radio-frequency double resonance devices, in which resonant linearly polarized light is used in the optical pumping and detection processes. We extend previous work by presenting algebraic results which are valid for atomic states with arbitrary angular momenta, arbitrary rf intensities, and arbitrary geometries. The only restriction made is the assumption of low light intensity. The results are discussed in view of their use in optical magnetometers.

PACS numbers: 32.60.+i, 32.30.Dx, 07.55.Ge, 33.40.+f

I. INTRODUCTION

Since the 1950s the combination of resonant optical excitation and magnetic resonance has been an extremely valuable tool for atomic spectroscopy. This double resonance technique [1] has not only proven useful for investigating atomic structure, for measuring properties of atoms, their constituents, and their interactions, but has also led to important applications in atom cooling, optically pumped frequency standards, and optical magnetometers.

Magnetometers based on double resonance in atomic samples measure the modulus of an externally applied magnetic field B_0 via the Larmor precession frequency of the sample's magnetization in that field [2, 3]. The sample is typically a vapor of paramagnetic atoms (or diamagnetic atoms excited to a metastable state with an orbital angular momentum) sealed in a glass cell. A macroscopic magnetization is created in the vapor by optical pumping with polarized resonance radiation. The magnetization precesses in the magnetic field B_0 to be measured (referred to as the *o* set field) and that precession is driven by a (much weaker) magnetic field $B_1(t)$ (referred to as the *rf* field), co-rotating with the magnetization around the *o* set field.

Since the optical properties of the medium, characterized by its complex index of refraction, depend on its spin polarization, the driven magnetization will induce periodic modulations of those properties [4, 5], which are then detected. In most applications, the same light beam used to polarize the medium is also used to monitor the oscillations by measuring either the power or the polarization state of the transmitted beam. The frequency of the induced oscillations coincides with the oscillation frequency ω of the *rf* field, and their amplitude depends in a resonant way on the detuning between ω and the

Larmor frequency $\omega_0 = \gamma_F B_0$ associated with the *o* set field. The Lande factor $\gamma_F = g_F \mu_B / \hbar$ is characteristic for the pumped atomic state with total angular momentum F .

Most practical double resonance devices rely on atomic orientation prepared by optical pumping with circularly polarized light. In this paper we present a theoretical study of the resonance signals obtained in double resonance spectroscopy using linearly polarized light. As shown first by Bell and Bloom [6] magnetic resonance in aligned media leads to signal modulations at the fundamental and at the second harmonic of the *rf* frequency. We derive algebraic expressions for the spectral line shapes of the in-phase and quadrature components of both signals and their orientation dependence. Previous theoretical treatments of such signals [7, 8] were restricted to specific angular momentum states ($J = 1$) or to low *rf* powers. The results presented here are more general in the sense that they apply to arbitrary spin systems and that they are valid for arbitrary *rf* power levels and for arbitrary orientations of B_0 with respect to the light polarization.

II. POLARIZED ATOMIC MEDIA

A. Atomic Multipole Moments

The density matrix of an ensemble of polarized atoms with angular momentum F can be expressed in terms of atomic multipole moments $m_{k,q}$ according to [9]

$$\hat{\rho}^F = \sum_{k=0}^F \sum_{q=-k}^k m_{k,q} T_q^{(k)}; \quad (1)$$

Electronic address: antoine.weis@unifr.ch

where the $T_q^{(k)}$ are standard irreducible tensor operators

$$T_q^{(k)}(F) = \sum_{M=F, M^0=F} \begin{pmatrix} F & 1 & F^0 \\ M & q & M^0 \end{pmatrix} T_q^{(k)}(F) \quad (2)$$

constructed from the angular momentum states $|F; M\rangle$, and where the multipole moments m_{kq} are defined by

$$m_{kq} = \frac{D}{E} T_q^{(k)y} = \text{Tr}(T_q^{(k)y}) \quad (3)$$

The three multipole moments $m_{k=1; q=-1; 0; +1}$ represent the orientation of the medium, while the five components $m_{k=2; q=-2; -1; 0; +1; +2}$ represent its alignment. The multipole moments $m_{k; q=0}$ are called longitudinal multipole moments and their value depends only on sublevel populations. The multipole moments $m_{k; q \neq 0}$ represent sublevel coherences and are called transverse moments. The representation of the atomic polarization in terms of multipole moments has a significant advantage over a representation in terms of sublevel populations and coherences. In principle, both representations require the same number of parameters for the complete description of the atomic ensemble. However, because electric dipole radiation couples only [10] to orientation ($k=1$) and alignment ($k=2$) it is sufficient to specify the corresponding $3+5=8$ multipole moments for the complete description of the system's optical properties. Moreover, specific light polarizations couple only to specific subsets of these 8 multipole moments, so that the use of the tensor formalism in systems with large angular momenta leads to a significant simplification of the mathematical treatment. In the case discussed here only the (real) multipole moment $m_{2,0}$ will be relevant. This approach therefore allows one to derive results valid for systems with arbitrary angular momenta.

A resonant circularly polarized laser beam interacting with an unpolarized atomic sample will create orientation ($k=1$, vector polarization) and alignment ($k=2$, tensor polarization) in the sample by optical pumping. The lowest order multipole that a linearly polarized light field can create is an atomic alignment. While only atomic states with $J=1/2$ can be oriented, the condition $J=1$ has to be fulfilled for the creation of an aligned state. Note that an alignment along the direction of light propagation can also be produced by pumping with unpolarized light [6, 11]. The ground state of alkali atoms has an electronic angular momentum $J=1/2$, which cannot be aligned. However, the hyperfine interaction with the nuclear spin splits the ground state into two hyperfine levels with total angular momenta $F=1/2, 3/2$, which can be aligned provided $F=3/2$. An alignment can therefore be prepared and/or detected only if the light source has a sufficient spectral resolution to excite a single hyperfine transition. In general the Doppler (and pressure) broadened spectra of discharge lamps, used in conventional optically pumped magnetometers (OPM), cannot be used to address individual hyperfine lines and hence

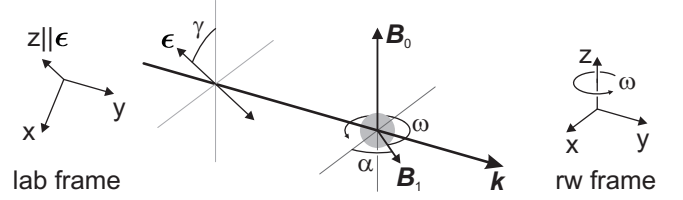


FIG. 1: Parametrization of the DROM geometry, in which B_1 is perpendicular to B_0 . The rotating wave (rw) frame and the rotating magnetic field B_1 are shown for one particular moment in time ($t=0$).

do not allow one to create nor to detect a ground state alignment. However, radiation from a narrowband laser can resolve the hyperfine structure and it is well known that a linearly polarized laser beam can create an atomic alignment.

B. DROMs and DRAMs

We will refer to an OPM based on atomic orientation as DROM (double resonance orientation magnetometer), while we will speak of DRAM (double resonance alignment magnetometer) when the magnetization has the symmetry of an atomic alignment. Most of the past research work on double resonance spectroscopy dealt with oriented vapors, although alignment induced by (unpolarized) lamp pumping in $J=1$ metastable states of ^4He was already reported in 1960/61 [6, 11]. In alkali atoms, alignment produced by lamp pumping can be observed using line splitting by the quadratic Zeeman effect [12] or isotope filtering [5, 12]. The latter technique is, however, restricted to Rb and cannot be applied to other alkalis. As mentioned above, linearly polarized laser radiation is an efficient means for producing alignment and a discussion of linearly polarized laser pumping in metastable ^4He can be found in [7, 13]. These authors have investigated several magnetometry techniques using both orientation and alignment signals and they observed magnetic resonances involving alignment using rf fields, light intensity modulation, polarization modulation, and frequency modulation. A variant of the latter technique (in which the transmitted light's polarization, instead of intensity, was measured) was realized with ^{87}Rb [14, 15].

III. MODEL CALCULATIONS

A. DRAM geometry

We will restrict the discussion to geometries in which the rf field B_1 is perpendicular to the offset field B_0 . Because the signals are independent of the orientation \mathbf{k} , the geometry of the problem is fully determined by $\mathbf{B}_0, \mathbf{B}_1$, and \mathbf{b} so that one can consider the parametrization shown

in Fig. 1, in which θ denotes the angle between the σ -set field and the light polarization [8]. The orientation dependence of the signal amplitudes is given by $\cos^2 \theta$, while the polar angle θ will lead to a phase shift in the time dependence of the oscillating signals (Sec. IV B).

In Fig. 1 we have applied the rotating wave approximation by decomposing the rf field into two counter-rotating fields, from which we have retained only the component co-rotating with the alignment. This component is shown in its position at time $t = 0$, thereby defining the time origin of the phases of the oscillating signal components. The magnetometer signals are calculated following the 3-step (prepare, evolve, probe) approach introduced in [16, 17] and discussed in detail in [18]. In the first step of this model (preparation) one assumes the existence of a given alignment in the atomic medium, without specifying how this alignment was created. Details of the preparation process (optical pumping, collisions with electrons or ions, spin exchange, etc) thus do not need to be known. In the second step (magnetic resonance) the initial alignment is allowed to evolve towards a steady state value determined by the interaction with the external fields and relaxation. Finally one considers in the third step (probing) how the steady state alignment affects a linearly polarized light beam traversing the medium. Strictly speaking this approach is only valid for pump-probe experiments, in which the atoms interact with spatially or temporally separated light fields and where the equilibrium of step 2 is reached "in the dark". However, as shown previously [16, 17] for level crossing signals the results obtained from the 3-step approach give an excellent description of experimental findings if the light intensity is sufficiently weak. Limitations of the model will be addressed in section III E.

B. Step 1: Alignment creation

We describe the alignment created by the preparation process in a coordinate frame where the quantization axis lies along the light polarization (lab frame in Fig. 1). In that frame the only non-vanishing alignment component created by optical pumping with linearly polarized light is the longitudinal multipole moment $m_{2,0}^{\text{ini}}$ which can be expressed in terms of the sublevel populations p_M as

$$m_{2,0}^{\text{ini}} = N_2(F) \sum_{M=-F}^F p_M \frac{3M^2 - F(F+1)}{2} ;$$

where $N_2(F)$ is a normalization constant [9]. In the presence of an σ -set field B_0 the alignment components perpendicular to B_0 will relax to zero yielding a steady state value of

$$m_{2,0}^{\text{eq}} = m_{2,0}^{\text{ini}} \frac{3 \cos^2 \theta}{2} \quad (4)$$

for the alignment along the magnetic field, given by the projection of $m_{2,0}^{\text{ini}}$ on the field direction. Note that this

steady state is reached only when the Larmor frequency is much larger than the transverse relaxation rates. This condition is well fulfilled for high-Q magnetic resonances while it is not met by zero-field level-crossing resonances (ground state Hanle effect, nonlinear Faraday effect [18]).

C. Step 2: Magnetic resonance

This step describes the magnetic resonance process, i.e., the evolution of the alignment under the combined actions of the magnetic fields B_0 , B_1 , and relaxation processes. It is described in a coordinate frame, which is related to the lab frame by a static rotation of θ around the y-axis and then by a dynamic rotation, at the frequency ω , around the new z-axis. In this frame, which we call the rotating wave frame (rw frame), the σ -set field B_0 is along z, while the rf field B_1 appears to be static and oriented at an angle θ with respect to the x-direction (see Fig 1). This is the usual field configuration for describing magnetic resonance processes. Note that $m_{2,0}^{\text{eq}}$ is not affected by the transformation to the rw frame. Due to the rotation of the coordinate frame, a fictitious magnetic field $B_F = \hbar \omega / g_F \mu_B$ appears in the rw frame, and the atoms see a total field $B_{\text{tot}} = B_1 \cos \theta + B_1 \sin \theta + (B_0 + \hbar \omega / g_F \mu_B) \hat{z}$.

The evolution of the system's density matrix is described by the Liouville equation

$$\frac{d}{dt} \rho = \frac{1}{\hbar} [H; \rho] - \rho / T_{\text{relax}} ; \quad (5)$$

with $H = \mu_B B_{\text{tot}}$, and where T_{relax} describes the relaxation processes. Inserting the multipole decomposition (1) into (5) yields the following equations of motion for the multipole moments $m_{2,q}$

$$\frac{d}{dt} m_{2,q} = \sum_{q'} O_{qq'}^{(2)} m_{2,q'} - m_{2,q} / T_{\text{relax}} \quad q = -2; -1; 0; 1; 2 ; \quad (6)$$

where $O_{qq'}^{(2)}$ is given by

$$O_{qq'}^{(2)} = \begin{pmatrix} 0 & 2i & i\hbar p_- & q \frac{0}{2} & 0 & 0 \\ i\hbar p_+ & q \frac{-3}{2} \hbar p_+ & i \frac{3}{2} \hbar p_- & q \frac{0}{2} & 0 & 0 \\ 0 & i \frac{3}{2} \hbar p_+ & q \frac{-3}{2} \hbar p_- & i \frac{3}{2} \hbar p_+ & 0 & 0 \\ 0 & 0 & i \frac{3}{2} \hbar p_+ & i & i\hbar p_+ & 2i \\ 0 & 0 & 0 & i\hbar p_+ & 2i & 0 \end{pmatrix} ;$$

in which $\hbar \omega_1 = g_F B_1$ is the Rabi frequency of the rf field, $p_{\pm} = \exp(\pm i\theta)$ are phase factors that describe the orientation of \mathbf{B}_1 in the xy-plane, and $\omega = \omega_0 + \omega_1$ is the detuning of the radio frequency ω with respect to the Larmor frequency ω_0 . The relaxation terms are given by

$$\begin{pmatrix} 0 \\ m_{2;2}^{\text{relax}} \\ m_{2;1}^{\text{relax}} \\ m_{2;0}^{\text{relax}} \\ m_{2;-1}^{\text{relax}} \\ m_{2;-2}^{\text{relax}} \end{pmatrix} = \begin{pmatrix} 1 & 0 & 0 & 0 & 0 \\ 0 & C & C & C & C \\ 0 & C & C & C & C \\ 0 & C & C & C & C \\ 0 & C & C & C & C \\ 0 & C & C & C & C \end{pmatrix} \begin{pmatrix} 0 \\ 2m_{2;2} \\ 1m_{2;1} \\ 0(m_{2;0}^{\text{eq}}) \\ 1m_{2;-1} \\ 2m_{2;-2} \end{pmatrix} + \begin{pmatrix} 1 \\ 0 \\ 0 \\ 0 \\ 0 \\ 0 \end{pmatrix} \quad (7)$$

where we assume that the multipole moments $m_{2;q}$ relax at rates $\gamma_{2;q}$. The transverse alignment components $m_{2;q \neq 0}$ relax towards a zero value, while the longitudinal component $m_{2;0}$ relaxes towards $m_{2;0}^{\text{eq}}$, introduced in step 1. Below, we present very general results for the case when all three relaxation rates are different, although it is well known that there are specific relations between those rates when the relaxation mechanism has specific rotational symmetries [19]. Equations 6 are a generalization of the well known Bloch equations

$$\frac{d}{dt} m_{1;q} = \sum_{q^0} X_{qq^0}^{(1)} m_{1;q^0} - m_{1;q}^{\text{relax}} \quad q = 1; 0; 1; \quad (8)$$

describing the evolution of the three orientation components $m_{1;q}$.

We have used a computer algebra software to determine algebraic expressions for the steady state ($d/dt m_{2;q} = 0$) solutions $m_{2;q}$ of (6). These solutions are then transformed back to the lab frame, by first applying a dynamic rotation at the rate ω around the z-axis, and then a static rotation by θ around the y-axis of the rf frame. In this way one can derive algebraic expressions for the time dependent multipole moments $m_{2;q}(t)$ in the lab frame.

D. Step 3: Alignment detection

In the third and final step, we calculate the effect the time dependent multipole moments have on the optical absorption coefficient of the medium. One can show that the absorption coefficient of a medium described by $m_{k;q}$ for linearly polarized light is proportional to

$$\frac{A_0}{P} = m_{0;0} + \frac{2}{3} A_2 m_{2;0}; \quad (9)$$

where the (analyzing power) A_k depends only on the states $|j_g; L_g; J_g; F_g\rangle$ and $|j_e; L_e; J_e; F_e\rangle$ coupled by the light. The multipole moments in (9) are defined with respect to a quantization axis oriented along the incident light polarization, which is the case in the lab frame, i.e., the frame in which the results of step 2 are expressed. The monopole moment $m_{0;0}$ describes the total population of the hyperfine ground state $|j_g; L_g; J_g; F_g\rangle$. We assume the optical transition to be closed and the light intensity to be so weak that excited state populations remain negligible, so that the monopole moment does not depend on time. The only time dependent (oscillating) component of the absorption coefficient is therefore

proportional to $m_{2;0}(t)$. We define the time dependent DRAM signal, normalized to the longitudinal alignment initially produced by the optical pumping, as

$$S(t) = \frac{m_{2;0}(t)}{m_{2;0}^{\text{ini}}}; \quad (10)$$

E. Validity of the three step approach

The three step approach is only valid if steady state conditions are reached in steps 1 and 2. This is fulfilled when the pump rate γ_p , at which alignment components are modified by the interaction with the light is negligible compared to the relaxation rates $\gamma_{2;q}$. This condition can be realized experimentally at low light powers, however, at the cost of a decreased signal to noise ratio. OPMs are known to perform best when γ_p is comparable to $\gamma_{2;q}$. The lowest order correction, taking the depolarization of light interactions into account, can be described by

$$\gamma_{2;q} \rightarrow \gamma_{2;q} + \gamma_p = \gamma_{2;q} + P_L; \quad (11)$$

where P_L is the laser power.

It is well known that substitution (11) is valid to all orders in P_L for a DROM in a spin 1/2 system [20], in which orientation is the only multipole moment that can be created. It is reasonable to assume that the same statement can be made for a DRAM in a spin 1 system in which alignment is the only multipole moment created and detected by the linearly polarized light. For angular momenta $F > 1$ the creation of higher order ($k > 2$) multipole moments and their transfer back to (detectable) $k = 2$ moments limits the validity of substitution (11) to low light powers.

IV. RESULTS

The calculation outlined above yields signals $S_1(t)$ and $S_{2!}(t)$ which are modulated at the rf frequency ω and at its second harmonic 2ω , and which can be written as

$$S_1(t) = h_1(\theta) [D_1 \cos(\omega t) + A_1 \sin(\omega t)]; \quad (12a)$$

$$S_{2!}(t) = h_{2!}(\theta) [A_{2!} \cos(2\omega t) + D_{2!} \sin(2\omega t)]; \quad (12b)$$

where the angular dependence of the signals $h_1(\theta)$ and $h_{2!}(\theta)$ (Fig. 2) is given by

$$h_1(\theta) = \frac{3}{2} \sin \theta \cos \theta - 3 \cos^2 \theta - 1 \quad (13a)$$

$$h_{2!}(\theta) = \frac{3}{4} \sin^2 \theta - 1 - 3 \cos^2 \theta; \quad (13b)$$

As stated earlier the orientation angle θ of the rf field appears as a phase shift. The in-phase and quadrature

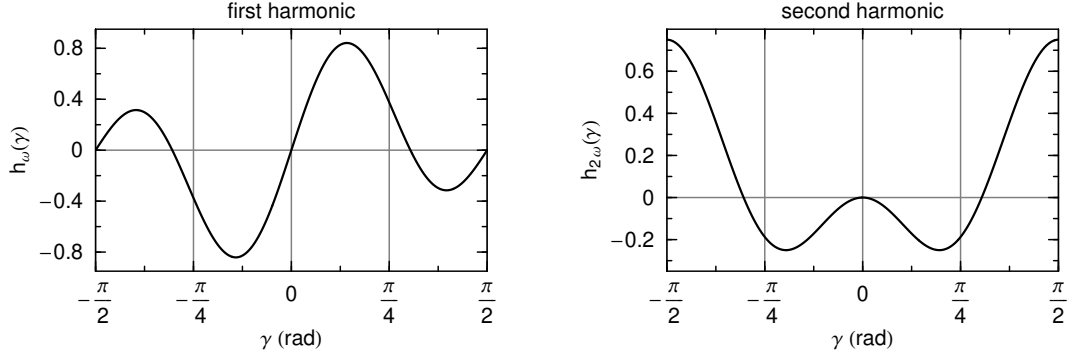


FIG. 2: Angular dependence of the first (h_1 , left) and second (h_2 , right) harmonic signals on the angle between the light polarization and the magnetic field B_0 .

components of the signal have both absorptive (A_1, A_2) and dispersive (D_1, D_2) lineshapes given by

$$D_1 = \frac{\omega_0^2 \gamma_1^2 + 4\gamma_2^2 \gamma_1^2}{Z}; \quad (14a)$$

$$A_1 = \frac{\omega_0^2 \gamma_1^2 + 4\gamma_2^2 \gamma_1^2}{Z}; \quad (14b)$$

$$D_2 = \frac{\omega_0^2 \gamma_1^2 (2\gamma_1 + \gamma_2)}{Z}; \quad (14c)$$

$$A_2 = \frac{\omega_0^2 \gamma_1^2 (2\gamma_1 + \gamma_2)}{Z}; \quad (14d)$$

with

$$Z = \omega_0^2 \gamma_1^2 + 4\gamma_2^2 \gamma_1^2 + \gamma_1^2 (2\gamma_0 + 3\gamma_2) + 4\gamma_2^2 (\gamma_0 + 3\gamma_1) \gamma_1^2 + (\gamma_0 + 3\gamma_2) \gamma_1^4; \quad (15)$$

Equations (14) and (15) can be simplified substantially if we assume an isotropic relaxation by setting $\gamma_0 = \gamma_1 = \gamma_2$. We will stick to this assumption in the following discussion since it does not change the general properties of the spectra. We further simplify the notation by introducing a dimensionless rf saturation parameter $S_{rf} = (\gamma_1^2)^2$ and a normalized detuning $x = \Delta/\gamma_1$. With these assumptions and definitions we obtain

$$D_1(x; S_{rf}) = \frac{x(1 - 2S_{rf} + 4x^2)}{(1 + S_{rf} + x^2)(1 + 4S_{rf} + 4x^2)}; \quad (16a)$$

$$A_1(x; S_{rf}) = \frac{1 + S_{rf} + 4x^2}{(1 + S_{rf} + x^2)(1 + 4S_{rf} + 4x^2)}; \quad (16b)$$

$$D_2(x; S_{rf}) = \frac{3xS_{rf}}{(1 + S_{rf} + x^2)(1 + 4S_{rf} + 4x^2)}; \quad (16c)$$

$$A_2(x; S_{rf}) = \frac{1 + S_{rf} - 2x^2}{(1 + S_{rf} + x^2)(1 + 4S_{rf} + 4x^2)}; \quad (16d)$$

In the following we will discuss in detail the different properties of the signals (12) with lineshapes (16).

A. Line shapes

For low rf intensities, i.e., for $S_{rf} \ll 1$, the lineshapes (16) reduce to

$$D_1(x; S_{rf} \ll 1) = \frac{x}{1 + x^2} S_{rf}; \quad (17a)$$

$$A_1(x; S_{rf} \ll 1) = \frac{1}{1 + x^2} S_{rf}; \quad (17b)$$

and

$$D_2(x; S_{rf} \ll 1) = \frac{3x}{(1 + x^2)(1 + 4x^2)} S_{rf}; \quad (18a)$$

$$A_2(x; S_{rf} \ll 1) = \frac{1 - 2x^2}{(1 + x^2)(1 + 4x^2)} S_{rf}; \quad (18b)$$

Expressions (13) and (17), correspond to results obtained in earlier work [7, 8].

The corresponding spectra can be seen in the leftmost columns of Figs. 3 and 4. These figures also show how the lineshapes of the absorptive and dispersive signals A_1, D_1, A_2 , and D_2 change with increasing rf intensity. A narrow additional spectral feature appears in the first harmonic signal for $S_{rf} > 0.5$. The origin of this structure can be explained as follows: the basic interaction of the rf field with the angular momentum is the coupling of adjacent Zeeman sublevels. The corresponding $M = 1$ coherences oscillate at the rf frequency ω and their detection by the light field constitutes the first harmonic signal. With increasing rf power, a further interaction of a $M = 1$ coherence with the rf field B_1 becomes possible and leads to the creation of a $M = 2$ coherence, whose oscillation produces the second harmonic signal. An additional interaction of the $M = 2$ coherence with the rf field produces both $M = 3$ and $M = 1$ coherences. While the former cannot be detected optically since linearly polarized light couples at most to $M = 2$ coherences, the latter directly contributes to the first harmonic signal. In this sense, the additional features can be understood as resulting from the creation of a $M = 2$ coherence by a second order interaction with the rf field,

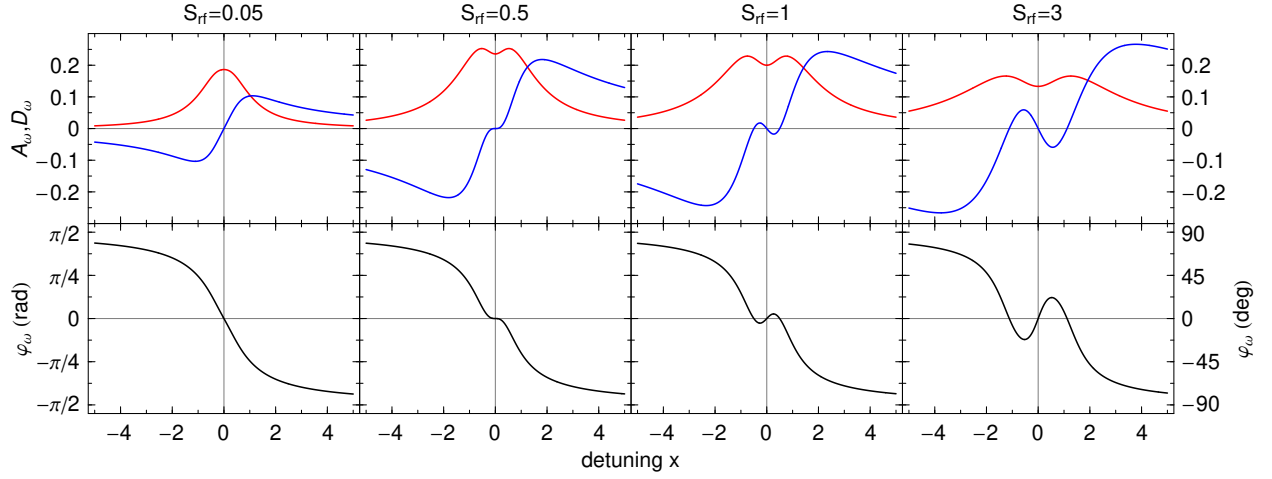


FIG. 3: (Color online) Top line: Line shapes of the absorptive (A_1) and dispersive (D_1) components of the first harmonic signal for different values of the rf saturation parameter S_{rf} . Bottom line: Shape of the phase signal φ_1 for the same values of S_{rf} . $x = (\omega - \omega_0)/\omega_0$ is the normalized detuning of the rf frequency ω with respect to the Larmor frequency ω_0 .

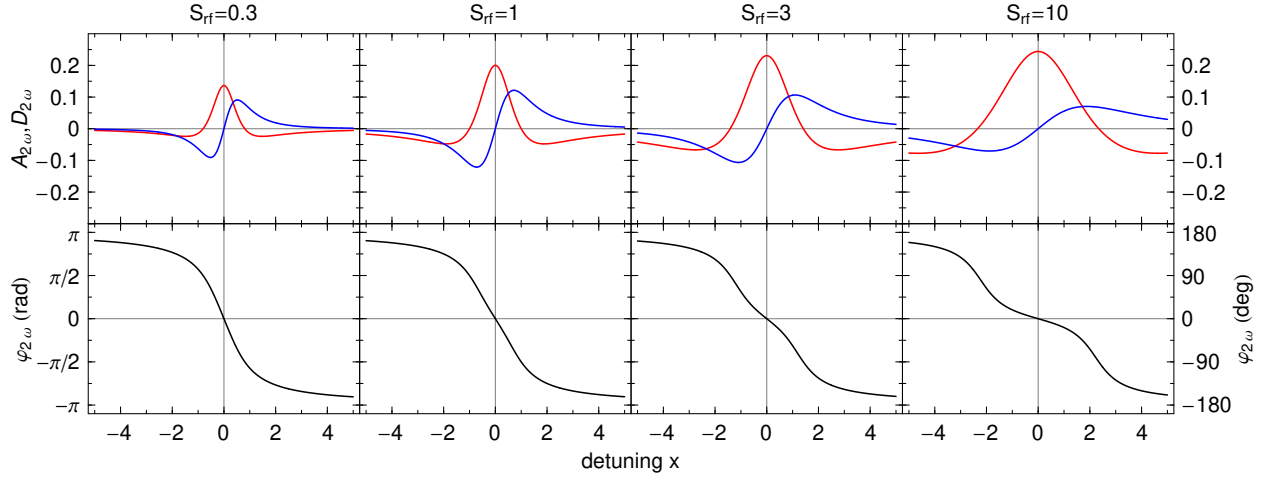


FIG. 4: (Color online) Top line: Line shapes of the absorptive (A_2) and dispersive (D_2) components of the second harmonic signal for different values of the rf saturation parameter S_{rf} . Bottom line: Shape of the phase signal φ_2 for the same values of S_{rf} .

the evolution of that coherence in the offset field, and back-transfer to a $M = 1$ coherence by an additional interaction with the rf field followed by detection of that coherence at the first harmonic frequency ω_1 .

The additional narrow feature in the absorptive signal that appears at large rf intensities was already observed in the pioneering work by Colegrove and Franken on optically induced alignment [11]. Based on the results presented above the feature can be explained in terms of line superpositions. In fact, the expression for the absorptive first harmonic signal A_1 (Eq. 16b) can be rewritten as

$$A_1 = \frac{1 + S_{rf}}{1 + S_{rf} + x^2} \frac{P}{S_{rf}} - \frac{4S_{rf}}{1 + 4S_{rf} + 4x^2} \frac{P}{S_{rf}}; \quad (19)$$

i.e., as a superposition of two absorptive Lorentzian line shapes whose widths, for $S_{rf} \neq 0$, differ by a factor of

2, while they become equal for large values of S_{rf} . The appearance of the central dip is a consequence of the different rates at which the contributions saturate with increasing S_{rf} . At low rf powers, the amplitudes of the two contributions to the first harmonic signals (19) grow as $S_{rf}^{1/2} / \omega_1$ and $S_{rf}^{3/2} / \omega_1^3$ respectively, which reflects that these resonances correspond to first and third order processes as discussed above. The second harmonic signals (Eqs. 18a, 18b), on the other hand, grow as ω_1^2 , which reflects their second order nature.

The dependence of the line widths, i.e., the frequency separation ω_{FW} of the maxima and minima of the dispersive signals D_1 and D_2 on S_{rf} can be inferred from the derivatives of (16a) and (16c). The dispersive line shape of the second harmonic signal D_2 is thus 2.6 times narrower than the corresponding first harmonic signal.

B. The phase of the signals

We define the phases ϕ_1 , (ϕ_2) of the first and second harmonic signals as the phase difference between $S_1(t)$ ($S_2(t)$) and oscillations that are proportional to $\cos t$ ($\cos 2t$) respectively. This definition is motivated by the fact that the rf field in the lab frame is proportional to $\cos t$. As an alternative to the parameterization of the signals in terms of in-phase and quadrature components (Eq.12) one can write $S_1(t)$ and $S_2(t)$ in terms of moduli R_1 , R_2 and phases ϕ_1 , ϕ_2 according to

$$S_1 = h_1(\alpha) R_1(x; S_{rf}) \cos[\omega t + \phi_1(x; S_{rf})]; \quad (20a)$$

$$S_2 = h_2(\alpha) R_2(x; S_{rf}) \cos[2\omega t + \phi_2(x; S_{rf})]; \quad (20b)$$

with

$$\phi_1 = \arctan \frac{A_1(x; S_{rf})}{D_1(x; S_{rf})} \quad (21)$$

$$\phi_2 = \arctan \frac{D_2(x; S_{rf})}{A_2(x; S_{rf})} \quad (22)$$

A dualphase lock-in amplifier can be used to extract the ϕ 's from the signal. Such amplifiers usually allow one to apply an offset phase ϕ_{os} to the signal which then adds to ϕ . For stabilization purposes, it is practical to choose that offset phase such that the total phase vanishes at the center of the resonance $\phi_1(x=0) = \phi_2(x=0) = 0$. This choice avoids phase discontinuities and provides a signal $\phi(x)/x$ (for $x \ll 1$) that is proportional to magnetic field changes near the center of the resonance. In the parameterization defined above this can be realized simultaneously for both signals when $\phi_1 + \phi_{os} = \phi_2 = 2$. In that case the phase signals take the form

$$\phi_1 = \arctan x \frac{1 - 2S_{rf} + 4x^2}{1 + S_{rf} + 4x^2}; \quad (23a)$$

$$\phi_2 = \arctan \frac{3x}{1 + S_{rf} - 2x^2}; \quad (23b)$$

Examples of $\phi_1(x)$ and $\phi_2(x)$ for different values of S_{rf} are shown in Figs. 3 and 4 respectively.

The phase of the first harmonic signal ϕ_1 (Eq. 23a) for low rf power ($S_{rf} \ll 1$) is identical to the phase of an orientation based magnetic resonance signal. Conversely to that DROM phase, which does not depend on S_{rf} , the DRAM phases ϕ_1 and ϕ_2 depend on S_{rf} , and ϕ_1 even changes the sign of its slope at $S_{rf} = 1/2$. Note that ϕ_2 makes a total phase swing of 2π across the resonance, while ϕ_1 swings only by π .

V. MAGNETOMETRY CONSIDERATIONS

There are two modes of OPM operation, the self-oscillating mode and the free running mode, which differ in the way the magnetic field value is extracted from the signals described above. Self-oscillating (or phase stabilized) magnetometers use feedback to keep the driving

frequency ω equal to ω_0 , and in such magnetometers, ω is measured with a frequency counter [21]. We will not discuss the self-oscillating mode in detail since the feedback is difficult to describe analytically. Instead, we discuss the free-running mode which yields an identical magnetic field sensitivity. The goal of the following discussion is not the derivation of absolute field sensitivities, but rather a comparison of the relative magnetometric sensitivities that one can expect from the first and second harmonic signals.

As a free-running magnetometer application we consider the recording of signal changes induced by variations of the offset field B_0 while the rf frequency ω is kept constant. Either the dispersive signals D_1 and D_2 (Eqs. 16a, 16c) or the phase signals ϕ_1 and ϕ_2 (Eqs. 23a, 23b) can be used as discriminating signals as they both feature a linear dependence on B_0 changes near the center of the resonance ($x = 0$).

The resolution with which field changes can be detected is limited by noise processes such as photon shot-noise, electron shotnoise (in a photodiode), and spin projection noise, all of which have a white noise spectrum. We specify the magnetometric sensitivity in terms of the noise equivalent magnetic field (NEM) [22, 23], which is the amplitude B^{NEM} of field fluctuations which induce fluctuations of the (dispersive) signal $S(B_0)$ that are equal to the signal noise S :

$$B^{NEM} = S / (dS/dB_0|_{x=0}) \quad (1)$$

One can show that for a given noise level of the modulated signal one obtains the same NEM either from the demodulated signal $S = D_1$ (D_2) or from the demodulated signals $S = \phi_1$ (ϕ_2). The minimal value of B^{NEM} is thus obtained under conditions which maximize h_1 , h_2 and h_2/h_1 , where the (on resonance) slopes s_1 and s_2 are given by

$$s_1 = \frac{dD_1}{dx} \Big|_{x=0} = \frac{(1 - 2S_{rf})^2 S_{rf}}{(1 + S_{rf})(1 + 4S_{rf})}; \quad (24a)$$

$$s_2 = \frac{dD_2}{dx} \Big|_{x=0} = \frac{3S_{rf}}{(1 + S_{rf})(1 + 4S_{rf})}; \quad (24b)$$

Figure 5 shows their dependence on the rf intensity. The zero crossing of the slope of the first harmonic signal at $S_{rf} = 0.5$ marks the emergence of the narrow central feature in Fig. 4.

The maximal sensitivity (minimal $B^{NEM}_{1,2}$) is achieved by choosing a geometry which maximizes h_1 and h_2 , and an rf intensity, which maximizes s_1 and s_2 . For the first harmonic signal one finds $\max[h_1, |s_1|] = 0.141$ for $\alpha = 25.5$ degrees and $S_{rf} = 0.079$, while for the second harmonic signal one has $\max[h_2, |s_2|] = 0.25$ for $\alpha = 90$ degrees and $S_{rf} = 0.5$. Under optimized geometrical and rf power conditions and for a given noise level the second harmonic signal is thus expected to yield a 1.8 times higher sensitivity to magnetic field changes than the first harmonic signal.

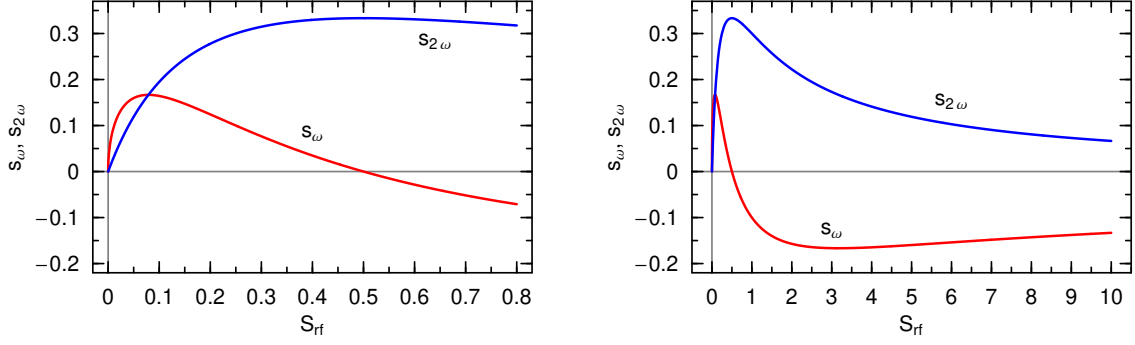


FIG. 5: (Color online) Slopes $s_{1,2}$ of the dispersive signals on resonance ($x = 0$) as a function of the rf saturation parameter for two different ranges of S_{rf} .

VI. SUMMARY AND CONCLUSION

We have presented a general theoretical framework for the calculation of optical rf double resonance signals that can be easily applied to oriented or aligned atomic media. The theory yields analytical results with a broad range of validity, and is only limited by the assumption of low light power.

DRAMs, i.e., magnetometers that use linearly polarized light, present several potential advantages over the well known DROM scheme:

Line widths: The line shapes of the second harmonic DRAM signal have significantly narrower linewidths than the DROM signal under identical conditions. Narrow linewidths potentially increase their magnetometric sensitivity and suppress systematic errors in optical magnetometers due to long term baseline drifts [24].

Light shift: In DROM devices the interaction of the atom with the circularly polarized laser light leads to M -dependent energy shifts (vector light shift) of the sublevels $|F, M\rangle$ when the laser frequency is not centered on the optical resonance line. In that case, power and frequency fluctuations of the laser magnetic field fluctuations, thereby limiting their magnetometric performance. In the DRAM device the linearly polarized light produces a tensor light shift [25] depending on M^2 , which does not have the characteristics of the Zeeman interaction and will therefore not affect their magnetometric performance.

Geometry: The DROM scheme achieves a maximal sensitivity for $\theta = 45^\circ$. The 45 degree angle that the laser beam has to make with the magnetic field seriously limits applications which call for a compact arrangement of multiple sensors. In multi-channel devices, as required, e.g., for cardiac magnetic measurements [26], the use of the DRAM signals offers the advantage that the laser beam can

be oriented either parallel or perpendicular to the offset field.

Vector magnetometry: Both the DROM and the DRAM devices are scalar magnetometers and their resonance frequency measures B_0 . However, the DRAM signals can be used to realize a vector magnetometer, since the ratio of R_2/R_1 is proportional to $\tan \theta$, for all values of S_{rf} . The knowledge of B_0 and θ locates B_0 on a cone and the variation of the signal with θ , obtained by rotating the polarizer, will determine the polar angle of B_0 on the cone. In this way the DRAM scheme can be used to infer all three vector components of the field.

Relaxation: We are in the process of performing extensive experimental studies of the DRAM properties in paraffin-coated cesium cells [27]. First results indicate that a description of the signals using three independent relaxation rates (Eqs. 14) is required to describe the experimental lineshapes in detail. The DRAM signals thus seem to offer a convenient way for studying spin relaxation processes in aligned media.

Signal noise: Diode lasers are convenient light sources for double resonance experiments. However, they often feature a $1/f$ (flicker) intensity noise at low frequencies that turns into the white shot noise level at higher frequencies. The detection of D_2 and A_2 at twice the Larmor frequency makes it easier to operate in a region where the laser noise is less affected by flicker noise.

Cs OPMs in the DROM geometry have a shot noise limited sensitivity of $10 \text{ fT}/\text{Hz}^{1/2}$ [23]. A direct experimental comparison of DRAM and DROM magnetometers is currently underway in our laboratory. This study will show if the potential advantages can be realized in practice.

Acknowledgments

The authors thank P. Knowles and G. Di Domenico for useful discussions and a critical reading of the manuscript. One of us (A.S.P.) acknowledges financial

support by the Swiss Heart Foundation. This work was supported by grant Nr. 205321-105597 from the Swiss National Science Foundation and by grant Nr. 8057.1 LSPF-LS from the Swiss Innovation Promotion Agency, CTI.

-
- [1] J. Brosseau and F. Bitter, *Phys. Rev.* **86** (3), 308 (1952).
 - [2] A. L. Bloom, *Appl. Opt.* **1**, 61 (1962).
 - [3] E. B. Aleksandrov and V. A. Bonch-Bruyevich, *Opt. Eng.* **31**, 711 (1992).
 - [4] H. G. Dehmelt, *Phys. Rev.* **105** (5), 1924 (1957).
 - [5] B. S. Mathur, H. Y. Tang, and W. Happer, *Phys. Rev. A* **2**, 648 (1970).
 - [6] W. E. Bell and A. L. Bloom, *Phys. Rev. Lett.* **6**, 623 (1961).
 - [7] H. Gilles, B. Cheron, and J. Hamel, *J. Phys. II France* **2**, 781 (1992).
 - [8] B. Cheron, H. Gilles, J. Hamel, O. Moreau, and E. Noel, *J. Phys. III France* **7**, 1735 (1997).
 - [9] K. Blum, *Density Matrix Theory and Applications* (Plenum Press, New York, 1996).
 - [10] W. Happer, *Rev. Mod. Phys.* **44**, 169 (1972).
 - [11] F. D. Colegrove and P. A. Franken, *Phys. Rev.* **119** (2), 680 (1960).
 - [12] E. B. Aleksandrov and M. V. Balabas, *Opt. Spectrosc.* **69**, 4 (1990).
 - [13] H. Gilles, J. Hamel, and B. Cheron, *Rev. Sci. Instr.* **72**, 2253 (2001).
 - [14] D. Budker, D. F. Kimball, S. M. Rochester, V. V. Yashchuk, and M. Zolotarev, *Phys. Rev. A* **62**, 043403 (2000).
 - [15] D. Budker, D. F. Kimball, V. V. Yashchuk, and M. Zolotarev, *Phys. Rev. A* **65**, 055403 (2002).
 - [16] A. Weis, J. Wurster, and S. I. Kanorski, *J. Opt. Soc. Am. B* **10**, 716 (1993).
 - [17] A. W. S. I. Kanorsky, J. Wurster, and T. W. Hansch, *Phys. Rev.* **47**, 1220 (1993).
 - [18] D. Budker, W. Gawlik, D. F. Kimball, S. M. Rochester, V. V. Yashchuk, and A. Weis, *Rev. Mod. Phys.* **74**, 1153 (2002).
 - [19] W. Happer, *Phys. Rev. B* **1**, 2203 (1970).
 - [20] N. Tsukada, T. Yabuzaki, and T. Ogawa, *J. Phys. Soc. Jap.* **11**, 698 (1972).
 - [21] S. G. Roeger, G. Bison, P. E. Knowles, and A. Weis, *Eur. Phys. J. Appl. Phys.* **33**, 221 (2006).
 - [22] G. Bison, R. Wynands, and A. Weis, *J. Opt. Soc. Am. B* **22**, 77 (2005).
 - [23] S. G. Roeger, G. Bison, J.-L. Schenker, R. Wynands, and A. Weis, *Eur. Phys. J. D* **38**, 239 (2006).
 - [24] E. B. Aleksandrov, A. S. Pazgalev, and J. L. Rasson, *Opt. Spectrosc.* **82**, 14 (1997).
 - [25] B. Mathur, H. Tang, and W. Happer, *Phys. Rev.* **171**, 11 (1968).
 - [26] G. Bison, R. Wynands, and A. Weis, *Opt. Expr.* **11**, 904 (2003).
 - [27] G. Di Domenico, G. Bison, S. G. Roeger, P. Knowles, A. S. Pazgalev, M. Rebetez, and A. Weis, to be published (2006).